ACS OMEGA

http://pubs.acs.org/journal/acsodf

Article

Ionic Liquid Mixtures for Direct Air Capture: High CO_2 Permeation Driven by Superior CO_2 Absorption with Lower Absolute Enthalpy

Yuki Kohno, Mitsuhiro Kanakubo, Masao Iwaya, Yo Yamato, and Takashi Makino*

Cite This: *ACS Omega* 2022, 7, 42155−42162

Read Online

ACCESS | Metrics & More | Article Recommendations | Supporting Information

ABSTRACT: This paper reports a series of liquid materials suitable for use as high-performance separation membranes in direct air capture. Upon mixing two ionic liquids (ILs), namely *N*-(2-aminoethyl)ethanolamine-based IL ([AEEA][X]) and 1-ethyl-3-methylimidazolium acetate ([emim][AcO]), the resulting mixtures with a specific range of their composition showed higher CO_2 absorption rates, larger CO_2 solubilities, and lower absolute enthalpies of CO_2 absorption compared to those of single ILs. NMR spectroscopy of the IL mixture after exposure to $^{13}CO_2$ allowed elucidation of the chemisorbed species, wherein [AEEA][X] reacts with CO_2 to form CO_2−[AEEA]$^+$ complexes stabilized by hydrogen bonding with acetate anions. Supported IL membranes composed of [AEEA][X]/[emim][AcO] mixtures were then fabricated, and the membrane with a suitable mixing ratio showed a CO_2 permeability of 25,983 Barrer and a CO_2/N_2 selectivity of 10,059 at 313.2 K and an applied CO_2 partial pressure of 40 Pa without water vapor. These values are higher than those reported for known facilitated transport membranes.

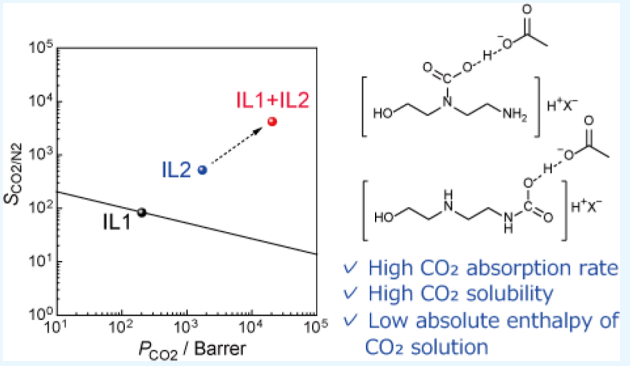

INTRODUCTION

The urgent need for strategies to reduce the global atmospheric concentrations of greenhouse gases has prompted action from governments and industries worldwide.[1,2] Post-combustion capture is typically considered for large point sources, such as coal- or gas-fired power plants, and industrial sources that produce large volumes of CO_2. However, these point sources account for only one-third to one-half of anthropogenic CO_2 emissions. Various recent scenarios have therefore demonstrated a requirement for the large-scale deployment of negative emission technologies,[3,4] which result in the net removal of greenhouse gases from the atmosphere. Among the various negative emission technologies reported to date, the development of a technology that can capture CO_2 from ambient air, referred to as "direct air capture" (DAC), is a challenge owing to the very low concentration of CO_2 in the atmosphere (i.e., ∼400 ppm).[5−7]

Membrane separation technologies are envisioned as one of the energy-efficient CO_2 separation technologies including DAC applications.[8−10] Facilitated transport membranes, in which mobile and/or fixed carriers are impregnated into the membrane matrices, are one of the options for DAC.[11] The facilitated transport of CO_2 through such membranes is accomplished as follows: the reactive carriers in the membranes react with CO_2 to produce CO_2-carrier complexes, which are then transported across the membranes. On the permeate side, the back reaction reversibly occurs at the low partial pressure of CO_2; eventually, CO_2 is released and the carrier is regenerated. The main challenge for such facilitated transport membranes for DAC applications is achieving a further improvement in the CO_2 permeability while maintaining, or even increasing, the CO_2/N_2 selectivity. Various properties of membrane materials influence the CO_2 permeability (i.e., the CO_2 solubility, the CO_2 absorption and desorption rate, the diffusivity (viscosity), and the enthalpy of solution of CO_2). One strategy to improve CO_2 permeability from the thermodynamic viewpoint is therefore to design carriers with high CO_2 solubilities and low absolute enthalpies of solution of CO_2, which should efficiently increase the mass of CO_2 transported through the membrane and readily desorb CO_2 at the permeate side owing to low absolute enthalpy.[12] However, it is difficult to accomplish both properties in a single material because a trade-off between the CO_2 solubility and enthalpy of solution is generally observed in such CO_2-sorptive materials.

The use of ionic liquids (ILs) as matrices for CO_2 separation membranes is regarded as a promising green technology because ILs have favorable properties, including negligibly low

Received: July 28, 2022
Accepted: October 20, 2022
Published: November 11, 2022

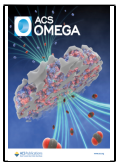

Scheme 1. Concept of IL Mixing for the Reversible Reaction of CO_2-Carrier Complexes in [emim][AcO]

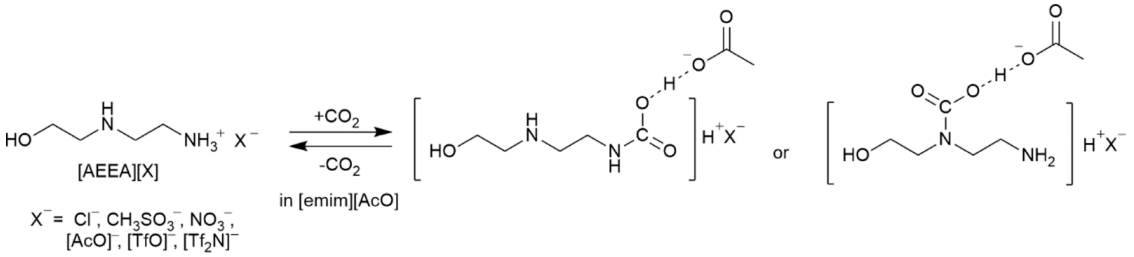

vapor pressure, high thermal/chemical stability, and low flammability.[13,14] Moreover, the structural design of the component ions of ILs allows precise control of their affinities toward CO_2. IL-based facilitated transport membranes, in which CO_2-reactive ILs are covalently tethered and/or physically impregnated in various membrane materials, have widely been investigated.[15,16] The CO_2-reactive ILs include cation-functionalized ILs with amino group on the cation,[17] amino acid ILs,[18−20] 2-cyanopyrrolide-type IL,[21] and carboxylate-type ILs.[22,23] Matsuyama and co-workers investigated various facilitated transport membranes using CO_2-reactive ILs (e.g., tetra-*n*-butylphosphonium-based amino acid ILs with L-glycinate, L-alaninate, L-serinate, and L-prolinate as anions), and some of these exhibited CO_2 permeability and CO_2/N_2 selectivity above the Robeson upper bounds.[19]

Previously, we measured the CO_2 solubility and the corresponding thermodynamic parameters for a series of carboxylate-type ILs with ether groups on the anions.[24] These ILs were revealed to possess lower absolute enthalpy of solution of CO_2 compared to well-known aqueous monoethanolamine solutions and thus are capable of desorbing CO_2 under mild temperature conditions below 100 °C. Although the structural design of the abovementioned "pure" ILs for specific applications is effective, the incorporation of functional groups into the ions tends to result in inferior liquid properties (e.g., higher viscosities and lower thermal stabilities). Instead, the mixing of multiple ILs can be a more practical means to fine-tune their properties than the structural design of pure ILs.[25] When considering the fine control of the affinity of IL mixtures toward CO_2, the suitable mixing of ILs (e.g., CO_2-reactive ILs and other ILs) should result in the discovery of unprecedented and superior liquid materials. However, the effect of mixing ILs on CO_2 separation performance has not been fully explored, presumably because of the complexity of the mixed systems compared to single IL systems.

We herein report the production of a new type of liquid material for DAC applications by mixing two ILs, namely *N*-(2-aminoethyl)ethanolamine-based IL ([AEEA][X]) and 1-ethyl-3-methylimidazolium acetate ([emim][AcO]). [AEEA][X] is expected to act as a CO_2 carrier, whereas the Lewis basic [emim][AcO] should stabilize zwitterion/carbamic acid species that exhibit relatively low absolute enthalpy of solution as compared to carbamate species (Scheme 1). Supported IL membranes (SILMs) are then fabricated and their CO_2/N_2 permselectivities are investigated in comparison with those of previously reported membrane materials.

EXPERIMENTAL SECTION

Synthesis of the ILs. The $[AEEA]^+$-based ILs used in this study ([AEEA][X]) were prepared by the neutralization of AEEA with equimolar amounts of the corresponding acids, as reported previously.[26] For example, in the preparation of $[AEEA][Tf_2N]$ ($[Tf_2N]$: bis(trifluoromethanesulfonyl)imide), AEEA and $H[Tf_2N]$ were mixed in water at a molar ratio of 1.0:1.0 while cooling the solution in an ice bath, and subsequently, the solution was allowed to stir for ≥2 h. After this time, the water was evaporated with a rotary evaporator, and the sample was dried in vacuo to obtain $[AEEA][Tf_2N]$.

Measurement of the CO_2 Solubility and Initial CO_2 Absorption Rate. The experimental apparatus used was the same as reported in the previous study except for the pressure transducer (Druck, IDOS UPM, USA).[27] The uncertainties of the pressure and the temperature were 10 Pa and 0.02 K, respectively. The high-pressure cell containing the desired amount of IL was attached to the experimental apparatus, and the apparatus was evacuated to remove volatile compounds. Subsequently, the apparatus was immersed in the thermostated water bath equipped with a chiller to maintain the temperature. The procedure was divided into two steps. The first step involved the determination of the quantity of the gas component. Thus, the molar amount of CO_2 loaded ($n_{CO_2}^{i}$) was calculated from the molar volume of CO_2 at equilibrium and the inner volume of the gas reservoir, which was preliminarily calibrated at each temperature. The liquid phase was then agitated using a stirrer bar. When the pressure change became <1 Pa h^{-1}, it was assumed that the components were present as a two-phase equilibrium. The concentration of the IL in the CO_2 phase was negligibly small. The molar amount of CO_2 dissolved in the IL ($n_{CO_2}^{L}$) was calculated according to the following equation

$$n_{CO_2}^{L} = n_{CO_2}^{i} - \frac{V_{cell} - V^{L}}{V_m^{G}} \quad (1)$$

where V^L and V_m^G represent the volume of the IL phase and the molar volume of the CO_2 phase under certain conditions, respectively. V_m^G was obtained from NIST REFPROP Ver. 10.0. It was assumed that the volume of the liquid phase (V^L) did not change after the CO_2 absorption under the present conditions. The solubility in molarity scale (c_{CO_2}), in which the uncertainty of c_{CO_2} was estimated as 0.001 mol dm^{-3} was obtained as follows

$$c_{CO_2} = \frac{n_{CO_2}^{i}}{V^{L}} \quad (2)$$

The same apparatus was used to measure the CO_2 absorption rate. More specifically, the desired amount of IL was introduced into the stainless-steel cell, and the IL was subjected to vacuum to remove any volatile components. Subsequently, CO_2 (≤1 kPa) was introduced into the cylinder;

https://doi.org/10.1021/acsomega.2c04756
ACS Omega 2022, 7, 42155−42162

Table 1. CO_2 Absorption Rate (J_0), Absorption Amount (c_{CO_2}), Enthalpy of Solution of CO_2 (ΔH), and Viscosity after CO_2 Absorption (η_{CO2}) of [AEEA][Tf_2N]/[emim][AcO] (10/90 mol %), as Well as Those of the Individual ILs

ILs	J_0/mmol m^{-2} s^{-1}[a]	c_{CO2}/mol dm^{-3}[b]	ΔH/kJ (mol-CO_2)$^{-1}$[c]	η_{CO2}/mPa s
[AEEA][Tf_2N]/[emim][AcO] (10/90 by mol)	0.39	0.157	−54	85.5
[emim][AcO]	3.4×10^{-3}	0.048	−61	65.9
[AEEA][Tf_2N]	2.3×10^{-3}	0.001	−73[d]	521

[a] p_{CO_2} = 40 Pa. [b] p_{CO_2} = 100 Pa. [c] p_{CO_2} = 1 kPa. [d] p_{CO_2} = 101 kPa.

the IL was present in a large excess (≥2800 times, molar equivalents) compared to CO_2. After reaching a constant pressure and temperature (313.15 K), the valve was opened to begin the CO_2 absorption experiment. The initial CO_2 absorption rate at the beginning of CO_2 absorption, J_0 (mmol m^{-2} s^{-1}), was obtained from the pressure change (Δp) per unit time

$$J_0 = \frac{\Delta p V^G}{ART} \quad (3)$$

where A is the area of the gas−liquid interface (8.04 cm^2), V^G is the volume of the gas phase, R is the gas constant, and T is the temperature. V^G was obtained by subtracting the volume of the IL, V^L, from the volume of the cell, V_{cell}. During the measurement, the volume of the IL was assumed to be constant.

Analysis of the CO_2 Saturated IL Solution. The experimental apparatus and procedure to prepare the CO_2 saturated IL solution were as described elsewhere.[24] A desired amount of IL was weighed into a glass cell using an electrical balance (Mettler Toledo, XP5003S, USA). Then, the glass cell was immersed in a water bath, where the temperature was kept at 313.15 K. A pair of stainless-steel needles attached to a silicon cap was used for the inlet and outlet of gas. Pre-heated CO_2 standard gas (CO_2 concentration was 391 ppm) was very slowly blown through the needle under the pressure of 101 kPa. The standard gas was supplied for ∼96 h until the IL was saturated with CO_2. After that, the saturated solution was transferred to the viscometer (Anton Paar, Stabinger SVM 3000, Austria) by using an airtight syringe to avoid air exposure. The viscosity was measured at 313.15 K. In the same manner, we prepared the IL solution saturated with a $^{13}CO_2$ standard ($^{13}CO_2$ concentration was 398 ppm) or $^{13}CO_2$ gases to analyze the CO_2−IL complexes. The saturated solution was analyzed by NMR (JEOL Resonance, ECA-600, Japan, for the ^{13}C NMR with the inverse-gated decoupling sequence and Bruker Avance 400, USA, for the 2D NMR with the C−H COSY sequence).

An FTIR spectrometer (Thermo Fisher Scientific, Nicolet iS50, USA) equipped with an ATR unit (PIKE Technologies, GladiATR, USA) was used to analyze CO_2 saturated solutions under atmospheric pressure (∼101 kPa). ∼0.1 mL of the IL was placed in a stainless-steel cell attached to the ATR unit. The ATR unit was kept at 313 K during the measurement. N_2 was then supplied to the cell and the IR spectrum of the neat IL was obtained. After that, the CO_2 standard gases (CO_2 concentrations: 391 ppm and 1.049%) were flowed to obtain the IR spectrum of the CO_2 saturated ILs.

Enthalpy of solution of CO_2 (ΔH) was measured according to our previous study.[24] The weight of IL (w_2) transferred into a stainless-steel cell was determined using an electrical balance (Mettler Toledo, AL-204, USA). Then, the cell was attached to the calorimeter, and N_2 was supplied immediately through a pre-heating line using a mass flow controller. We measured a heat flow at regular intervals using a Calvet-type calorimeter (Setaram, μDSC7, France) at 313.15 K. The sample temperature was kept within ±0.01 K during the measurements. We assumed that the IL was thermally equilibrated when the change of heat flow was less than 0.01 mW h^{-1}. After that, we started the measurement of the enthalpy of solution of CO_2 by switching from N_2 to CO_2. An exothermic peak was observed when CO_2 was absorbed in the IL. The heat flow became almost constant after the IL was saturated with CO_2. The criterion for the saturation was the same as that for the thermal equilibration. The enthalpy of solution of CO_2 (ΔH) was calculated as

$$\Delta H = f\frac{S}{\alpha_1(w_2/M_2)} \quad (4)$$

where S is the integral of the exothermic peak, α_1 is the molar ratio of dissolved CO_2 to IL, M_2 is the molecular weight of IL, and f is the instrumental factor determined preliminarily. The uncertainty of ΔH is estimated to be less than 4% under the present conditions.

Measurement of the CO_2/N_2 Gas Permeability. The SILMs were prepared as follows. A hydrophilic PTFE membrane (Merck Millipore, JVWP04700, USA) was dipped into the IL under vacuum at 25 °C for 24 h. The PTFE filter had a pore size of 0.1 μm, a porosity of 80%, and a thickness of 30 μm. The excess IL on the filter surface was wiped up immediately before the measurement. The filling rate of each IL in the PTFE filter was calculated to be 98−99%, which is determined as a volume of IL loaded in a void of PTFE filter. The membrane thickness before and after loading the ILs was unchanged. The experimental apparatus employed for the gas separation measurements was as described in our previous report.[28] The SILM (47 mm in diameter) was placed on a stainless-steel cell with a porous hydrophobic PTFE filter (Advantec Co., T010A047A, Japan) as the support. The PTFE filter had a pore size of 0.1 μm, a porosity of 68%, and a thickness of 70 μm. The effective surface area was 13.2 cm^2 and the thickness of the membrane was measured using a micrometer. The feed gas was a CO_2/N_2 mixture with a CO_2 partial pressure of 40 Pa, while helium was used as the sweep gas. The atmospheric pressure was measured using a barometer (Druck, DPI150, USA). The flow rates of the feed and sweep gases were 400 and 20−150 cm^3 min^{-1}, respectively, and they were regulated using mass flow controllers (HORIBA STEC Inc., SEC-E40, Japan). In the present study, the feed and sweep gases did not contain water. The temperature was controlled within ±1 K during the measurement. The permeabilities of CO_2 and N_2 were evaluated based on the flow rates and the compositions. The flow rate was measured using a film flow meter (HORIBA STEC Inc., SF-1U). The composition was determined using a TCD gas chromatograph (Shimadzu Co., GC-8A, Japan).

https://doi.org/10.1021/acsomega.2c04756
ACS Omega 2022, 7, 42155−42162

RESULTS AND DISCUSSION

To investigate the effectiveness of mixing different ILs, [AEEA][Tf_2N] was mixed with [emim][AcO] in a molar composition of 10/90. The equilibrium and kinetic parameters for CO_2 absorption in the IL mixture were analyzed; more specifically, the initial CO_2 absorption rate (J_0), the CO_2 solubility (c_{CO_2}), the enthalpy of solution of CO_2 (ΔH), and the viscosity after CO_2 absorption (η_{CO_2}) for the IL mixture were measured, as were the corresponding values for each IL at 313.2 K (Table 1). The J_0 value, defined as the number of moles of CO_2 absorbed per unit area and time, was measured by tracing the pressure decay caused by CO_2 absorption, and the initial absorption rate was plotted against the CO_2 pressure. A typical pressure profile is presented in Figure S1. Immediately after the valve was opened, a pressure drop was observed owing to the expansion of the gas phase. This pressure drop was completed within approximately 1 s. In this measurement, the subsequent pressure drop was assumed to be the change associated with CO_2 absorption into the IL. This measurement was performed for different CO_2 partial pressure (Figure 1a). The initial CO_2 absorption rate at the beginning of CO_2 absorption, J_0 (mmol m^{-2} s^{-1}), was then calculated, and the J_0 at 40 Pa was obtained by extrapolation. It was found that the J_0 value of the IL mixture was 116 times higher than that of [emim][AcO] and 370 times higher than that of [AEEA][Tf_2N]. Subsequently, the c_{CO_2} value was determined from the pressure difference after reaching equilibrium using the same apparatus employed to measure the J_0 values. The c_{CO_2} was plotted as a function of the CO_2 partial pressure, as shown in Figure 1b. The values given in Table 1 were calculated by interpolation. Because the c_{CO_2} value of [AEEA][Tf_2N] at CO_2 pressure of 40 Pa was below the detection limit of our system, the values at a CO_2 pressure of 100 Pa were compared in this study. A higher c_{CO_2} was observed in the IL mixture than in the individual ILs, and the value increased upon increasing the CO_2 pressure. Next, the ΔH values for each sample were measured at the CO_2 pressure of 1 kPa. It was revealed that the IL mixture displayed a smaller ΔH value than the individual ILs. On the other hand, the η_{CO_2} value for the IL mixture after the absorption of CO_2 was slightly higher than that of [emim][AcO] and significantly lower than that of [AEEA][Tf_2N]. Because the higher viscosity results in a slower diffusivity of the components, the diffusion of the CO_2-carrier complexes in the IL mixture should not be faster than that of [emim][AcO].

To elucidate the chemical structures of the CO_2-carrier complexes in the IL mixtures, the $^{13}CO_2$-absorbed [AEEA]-[Tf_2N]/[emim][AcO] mixtures (CO_2 partial pressure = 40 Pa) were analyzed by NMR spectroscopy. Figure 2a shows the ^{13}C inverse-gated NMR spectra of the mixtures with different [AEEA][Tf_2N] compositions after $^{13}CO_2$ absorption. As a reference, the NMR spectra before $^{13}CO_2$ absorption are provided in Supporting Information (Figure S2). In the case of [emim][AcO] alone, the chemisorbed product was observed at 155 ppm. We previously analyzed the CO_2-chemisorbed products in various carboxylate-type ILs by ^1H and ^{13}C NMR spectroscopy.[24] The peak observed at 155 ppm was originated from the reaction between CO_2 and the 2-H position of the imidazolium cation. The C2 hydrogen released from [emim][AcO] was transferred to $[AcO]^-$ to form

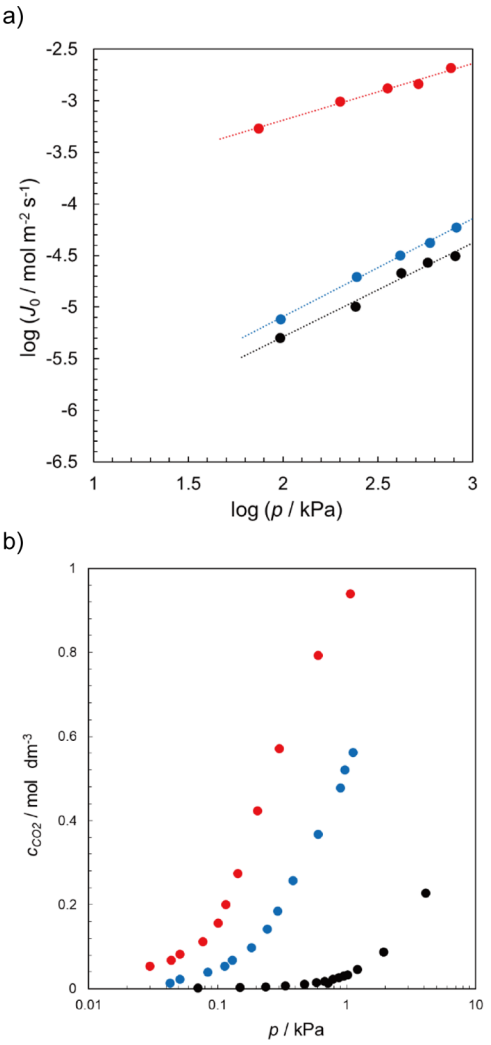

Figure 1. (a) Initial CO_2 absorption rate (J_0) against the CO_2 partial pressure; (b) CO_2 solubility (c_{CO_2}) in different ILs. Black circle/line: [AEEA][Tf_2N]; blue circle/line: [emim][AcO]; and red circle/line: [AEEA][Tf_2N]/[emim][AcO] (10/90 mol %).

carboxylic acids. Such a reaction mechanism was also supported by single-crystal X-ray structures of solid-state products.[29]

Upon mixing 10 mol % [AEEA][Tf_2N] in [emim][AcO], two CO_2-chemisorbed products were newly observed at 161 and 162 ppm, whereas the peak corresponding to the product with [emim][AcO] at 155 ppm reduced in intensity. Increasing the mixing ratio of [AEEA][Tf_2N] to 70 mol % resulted in a decrease in the amount of these products, and the spectrum for $^{13}CO_2$-absorbed [AEEA][Tf_2N] showed product peaks at ~164 ppm. The integrated intensities for these CO_2-chemisorbed products in the IL mixtures were then ordered according to the mixing ratios of [AEEA][Tf_2N] giving: 10 mol % (3.4) > 0 mol % (1.9) ≈ 70 mol % (1.9) > 100 mol % (0.15). This order is consistent with the equilibrium CO_2 absorption amounts of these mixtures. For the mixture containing 10 mol % [AEEA][Tf_2N], the ratio of the integral intensities for the different CO_2-chemisorbed products was 13:29:1 (i.e., at 162, 161, and 155 ppm).

To determine the molecular structures of these products, 2D NMR spectroscopy was performed. Figure 2b shows the C−H COSY spectrum of the $^{13}CO_2$-absorbed [AEEA][Tf_2N]/

https://doi.org/10.1021/acsomega.2c04756
ACS Omega 2022, 7, 42155−42162

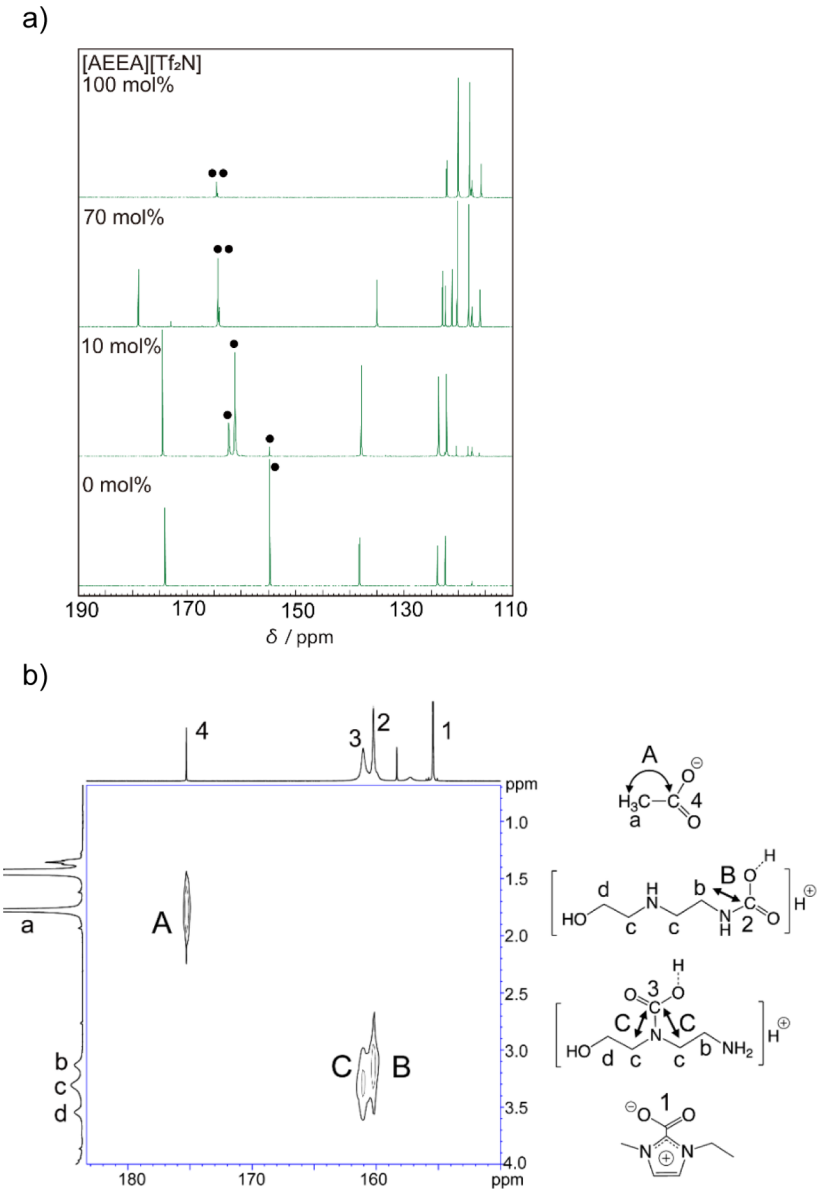

Figure 2. (a) ^{13}C inverse-gated NMR spectra of [AEEA][Tf_2N]/[emim][AcO] with different molar compositions of [AEEA][Tf_2N] after dissolving $^{13}CO_2$. Black dots represent carbon from $^{13}CO_2$. (b) C−H COSY spectrum of $^{13}CO_2$-absorbed [AEEA][Tf_2N]/[emim][AcO] (10/90 mol %) with elucidated structures.

[emim][AcO] mixture (10/90 mol %, CO_2 partial pressure = 40 Pa), in which three correlations were observed in the spectrum [i.e., 1.8−175 (A), 3.2−161 (B), and 3.3−162 ppm (C)]; the correlation (A) was assigned to the C−CH_3 moiety of $[AcO]^-$ (Figure 2b, inset A), and the correlations (B) and (C) were assigned to the CO_2-carrier complexes. More specifically, the correlation (B) was assigned to the CO_2−NH−CH_2 moiety of the CO_2-carrier complex, which originated from the reaction between CO_2 and the primary amino group of $[AEEA]^+$ (Figure 2b, inset B). In addition, the correlation (C) was as attributed to the CO_2−N−CH_2 moiety of the CO_2-carrier complex, which originated from the reaction between CO_2 and the secondary amino group of $[AEEA]^+$ (Figure 2b, inset C). It should be noted here that Kortunov et al. reported the NMR spectroscopic analyses of some CO_2-sorptive amines in [emim][AcO] and suggested that [emim][AcO] acted as a medium for these amines to form carbamic acid/zwitterionic species after reacting with CO_2.[30,31] Such CO_2-carrier complexes are more beneficial than carbamate species in terms of the CO_2 sorption amount per mol of amine (i.e., 1:1 CO_2/amine stoichiometry for carbamic acid/zwitterionic species and 1:2 CO_2/amine stoichiometry for carbamates).

In addition to NMR spectroscopy, IR spectroscopy[32] was employed to evaluate the [AEEA][Tf_2N]/[emim][AcO] mixture (10/90 mol %) and the individual ILs (Figure 3). Upon the exposure of [emim][AcO] to CO_2, the asymmetric vibration of the carboxylate group ($\nu_s(COO^-)$) was observed at 1666 cm^{-1}, and also the stretching vibration of the carboxylic acid group ($\nu_s(COOH)$) was observed as a shoulder peak upon increasing the CO_2 partial pressure (Figure 3a). In the case of the [AEEA][Tf_2N]/[emim][AcO] mixture, a broad peak corresponding to both $\nu_s(COOH)$ and $\nu_s(COO^-)$ was observed at ∼1620 to 1720 cm^{-1} (Figure 3b, red-highlighted region) at a CO_2 partial pressure of 40 Pa; the intensity of this peak increased as the CO_2 partial pressure was increased to 1

https://doi.org/10.1021/acsomega.2c04756
ACS Omega 2022, 7, 42155−42162

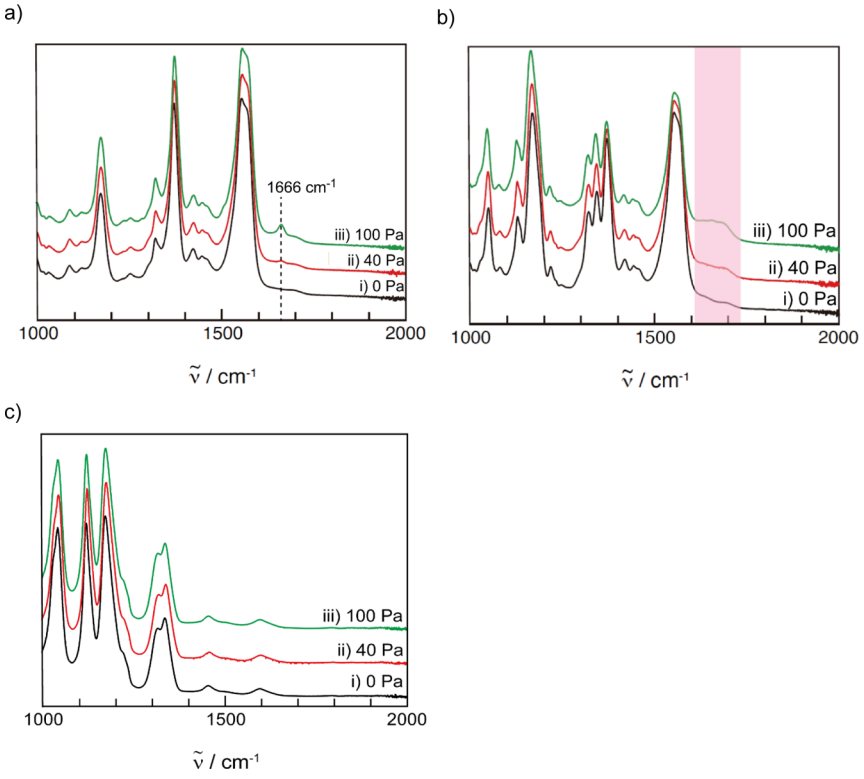

Figure 3. ATR-FTIR spectra for (a) [emim][AcO], (b) [AEEA][Tf_2N]/[emim][AcO] (10/90 mol %), and (c) [AEEA][Tf_2N] after exposure to CO_2 at different partial pressure.

kPa. For [AEEA][Tf_2N] only, no obvious change was observed in the spectra (Figure 3c). A possible interpretation of this result seen in the [AEEA][Tf_2N]/[emim][AcO] mixture is the presence of multiple structures derived from $[AcO]^-$/acetic acid species (e.g., the carbamic acid structure of CO_2-$[AEEA]^+$, and the acetic acid structure formed by proton transfer from CO_2-$[AEEA]^+$ to $[AcO]^-$ in [AEEA][Tf_2N]/[emim][AcO] with a low partial pressure of CO_2). Upon considering that the molar ratio of the CO_2−$[emim]^+$ complex was much less than the CO_2−$[AEEA]^+$ complexes, which was proved by ^{13}C NMR spectroscopy as mentioned above, the dominant proton source for acetic acid formation should be the CO_2−$[AEEA]^+$ complexes. The NMR and IR spectroscopy results therefore strongly suggest that the mechanistic pathway for chemisorption in [AEEA][Tf_2N]/[emim][AcO] is the reaction between CO_2 and the amino groups of [AEEA][Tf_2N], which is stabilized by $[AcO]^-$ via hydrogen bonding. Furthermore, the previous report showed that the formation of carbamate species and protonated amines resulted in a high absolute enthalpy of the solution of CO_2.[33] Based on this report, the carbamic acid/zwitterionic structure of the CO_2−$[AEEA]^+$ complexes in [AEEA][Tf_2N]/[emim][AcO] was assumed to lower the absolute enthalpy by suppressing both carbamate formation and proton transfer to amines.

Finally, the abovementioned IL mixtures were impregnated in a porous Teflon film to prepare SILMs, and the gas permeability from a mixed feed gas containing CO_2/N_2 (CO_2 partial pressure: 40 Pa) was analyzed. Figure 4a shows the CO_2 permeability values, p_{CO_2}, for the prepared SILMs with different [AEEA][Tf_2N] compositions. The p_{CO_2} value for [emim][AcO] alone was 1760 Barrer, although this value increased steeply to 20902 Barrer upon mixing with [AEEA][Tf_2N] in a molar composition of 10 mol %. A further increase in the molar composition of 70 mol % lowered the p_{CO_2} value (2332 Barrer), with [AEEA][Tf_2N] itself giving the lowest p_{CO_2} value among the various mixtures investigated (206 Barrer). In addition, the p_{N_2} value was almost constant over the investigated composition range. Figure 4b shows the CO_2/N_2 permeability selectivity (S_{CO_2/N_2}) as a function of p_{CO_2} (i.e., Robeson plots)[34] for the [AEEA]X/[emim][AcO] mixtures (10/90 mol %), where X^- corresponds to chloride (Cl^-), methanesulfonate ($CH_3SO_3^-$), $[AcO]^-$, nitrate (NO_3^-), triflate ($[TfO]^-$), and $[Tf_2N]^-$. As indicated, the [AEEA]X/[emim][AcO] mixtures displayed exceptionally high p_{CO_2} and S_{CO_2/N_2} values. Furthermore, the maximum values were observed for [AEEA][AcO]/[emim][AcO] at a molar ratio of 15:85 (p_{CO_2} = 25983 Barrer, S_{CO_2/N_2} = 10059). These values were higher than those previously reported for SILMs and other facilitated transported membranes under dry condition. As a typical reference, [P_{4444}][Pro],[19] a benchmark IL exhibiting high CO_2 permeability, was prepared in our laboratory and analyzed using the same experimental procedure to give a p_{CO_2} value of 22095 Barrer and a S_{CO_2/N_2} value of 4013, both of which were lower than those of [AEEA][AcO]/[emim][AcO].

Given the structural diversity of ILs, the abovementioned strategy (i.e., designing membrane materials by mixing plural ILs) would offer a new avenue for energy-efficient CO_2 separation processes. Currently, our group is investigating the structure−property relationships of IL mixtures with various structures. Future work will also collect a range of engineering data for applications in various DAC processes

https://doi.org/10.1021/acsomega.2c04756
ACS Omega 2022, 7, 42155−42162

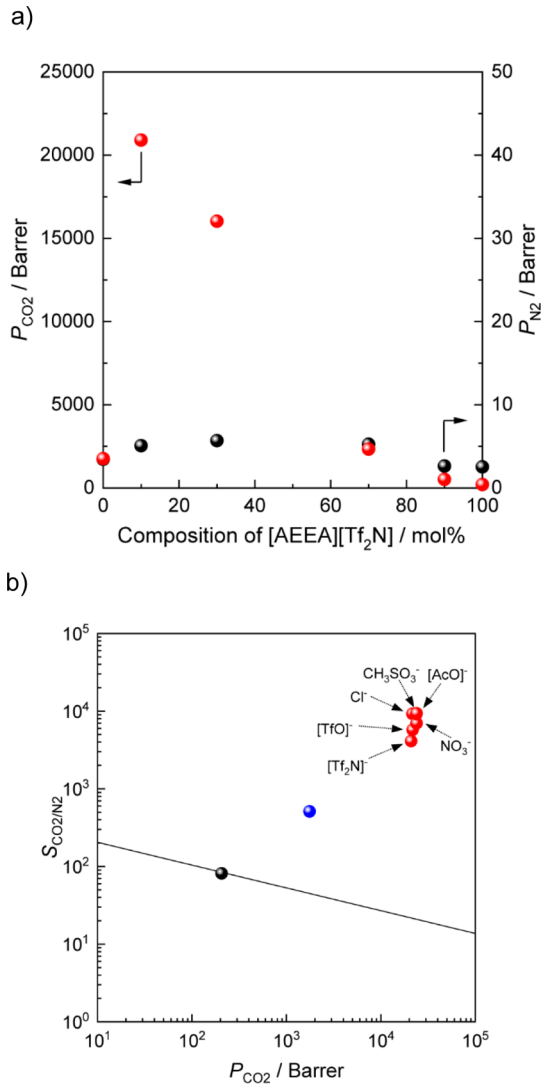

Figure 4. (a) CO_2/N_2 permeabilities (p_{CO_2} and p_{N_2}) for the supported [AEEA][Tf_2N]/[emim][AcO] membranes with different mixing compositions. (b) Robeson plot for the membranes composed of [AEEA][Tf_2N] (black circle), [emim][AcO] (blue circle), and [AEEA]X/[emim][AcO] (red circles). The solid line denotes the Robeson upper bounds.

(e.g., gas permeability properties under humid conditions, resistance to oxidative degradation).

CONCLUSIONS

It was found that IL mixtures comprising [AEEA]X/[emim]-[AcO] exhibit high CO_2 permeabilities and CO_2/N_2 permeability selectivity values even at a CO_2 feed partial pressure of 40 Pa without water vapor. The amount of CO_2 absorption and the CO_2 absorption rate by the IL mixtures was higher than those of the individual ILs, and the mixtures also exhibited the lowest absolute enthalpies of solution. The mechanistic pathway for chemisorption in the mixture was spectroscopically analyzed, and the dominant species were found to be the CO_2–$[AEEA]^+$ complexes, in which the zwitterion/carbamic acid species were assumed to be stabilized by $[AcO]^-$ via hydrogen bonding. These results therefore indicate that IL mixtures are promising new liquid membrane materials for DAC applications.

ASSOCIATED CONTENT

Supporting Information

The Supporting Information is available free of charge at https://pubs.acs.org/doi/10.1021/acsomega.2c04756.

Materials and NMR characterization of ILs (PDF)

AUTHOR INFORMATION

Corresponding Author

Takashi Makino − *National Institute of Advanced Industrial Science and Technology (AIST), Sendai 983-8551, Japan*; Email: makino.t@aist.go.jp

Authors

Yuki Kohno − *National Institute of Advanced Industrial Science and Technology (AIST), Sendai 983-8551, Japan*; orcid.org/0000-0003-3913-3444

Mitsuhiro Kanakubo − *National Institute of Advanced Industrial Science and Technology (AIST), Sendai 983-8551, Japan*

Masao Iwaya − *Daicel Corporation, Business Development Center, Innovation and Business Development Headquarters, Tokyo 108-0075, Japan*

Yo Yamato − *Daicel Corporation, Business Development Center, Innovation and Business Development Headquarters, Tokyo 108-0075, Japan*

Complete contact information is available at: https://pubs.acs.org/10.1021/acsomega.2c04756

Notes

The authors declare no competing financial interest.

ACKNOWLEDGMENTS

Financial support for this work was provided by the Adaptable and Seamless Technology Transfer Program through Target-driven R&D (A-STEP) from the Japan Science and Technology Agency (JST), no. JPMJTR203C.

REFERENCES

(1) Rogelj, J.; den Elzen, M.; Höhne, N.; Fransen, T.; Fekete, H.; Winkler, H.; Schaeffer, R.; Sha, F.; Riahi, K.; Meinshausen, M. Paris Agreement climate proposals need a boost to keep warming well below 2 °C. *Nature* **2016**, *534*, 631−639.

(2) Masson-Delmotte, V.; Zhai, P.; Pirani, A.; Connors, S. L.; Péan, C.; Berger, S.; Caud, N.; Chen, Y.; Goldfarb, L.; Gomis, M. I.et al.Climate Change 2021: The Physical Science Basis. *Contribution of Working Group I to the Sixth Assessment Report of the Intergovernmental Panel on Climate Change*; IPCC, 2021.

(3) Smith, P.; Davis, S. J.; Creutzig, F.; Fuss, S.; Minx, J.; Gabrielle, B.; Kato, E.; Jackson, R. B.; Cowie, A.; Kriegler, E.; et al. Biophysical and economic limits to negative CO_2 emissions. *Nat. Clim. Change* **2016**, *6*, 42−50.

(4) Minx, J. C.; Lamb, W. F.; Callaghan, M. W.; Fuss, S.; Hilaire, J.; Creutzig, F.; Amann, T.; Beringer, T.; de Oliveira Garcia, W.; Hartmann, J.; et al. Negative emissions-Part 1: Research landscape and synthesis. *Environ. Res. Lett.* **2018**, *13*, 063001.

(5) Shi, X.; Xiao, H.; Azarabadi, H.; Song, J.; Wu, X.; Chen, X.; Lackner, K. S. Sorbents for the Direct Capture of CO_2 from Ambient Air. *Angew. Chem., Int. Ed.* **2020**, *59*, 6984−7006.

(6) Sanz-Pérez, E. S.; Murdock, C. R.; Didas, S. A.; Jones, C. W. Direct Capture of CO_2 from Ambient Air. *Chem. Rev.* **2016**, *116*, 11840−11876.

(7) Fasihi, M.; Efimova, O.; Breyer, C. Techno-economic assessment of CO_2 direct air capture plants. *J. Clean. Prod.* **2019**, *224*, 957−980.

(8) Fujikawa, S.; Selyanchyn, R. Direct air capture by membranes. *MRS Bull.* **2022**, *47*, 416−423.
(9) Castro-Muñoz, R.; Zamidi Ahmad, M. Z.; Malankowska, M.; Coronas, J. A new relevant membrane application: CO_2 direct air capture (DAC). *J. Chem. Eng. J.* **2022**, *446*, 137047.
(10) Castel, C.; Bounaceur, R.; Favre, E. Membrane Process for Direct Carbon Dioxide Capture from Air: Possibilities and Limitations. *Front. Chem. Eng.* **2021**, *3*, 668867.
(11) Rahaman, M. S. A.; Zhang, L.; Cheng, L.-H.; Xu, X.-H.; Chen, H.-L. Capturing carbon dioxide from air using a fixed carrier facilitated transport membrane. *RSC Adv.* **2012**, *2*, 9165−9172.
(12) Otani, A.; Zhang, Y.; Matsuki, T.; Kamio, E.; Matsuyama, H.; Maginn, E. J. Molecular Design of High CO_2 reactivity and Low Viscosity Ionic Liquids for CO_2 Separative Facilitated Transport Membranes. *Ind. Eng. Chem. Res.* **2016**, *55*, 2821−2830.
(13) Bara, J. E.; Carlisle, T. K.; Gabriel, C. J.; Camper, D.; Finotello, A.; Gin, D. L.; Noble, R. D. Guide to CO_2 Separations in Imidazolium-Based Room-Temperature Ionic Liquids. *Ind. Eng. Chem. Res.* **2009**, *48*, 2739−2751.
(14) Scovazzo, P. Determination of the upper limits, benchmarks, and critical properties for gas separations using stabilized room temperature ionic liquid membranes (SILMs) for the purpose of guiding future research. *J. Membr. Sci.* **2009**, *343*, 199−211.
(15) Gao, H.; Bai, L.; Han, J.; Yang, B.; Zhang, S.; Zhang, X. Functionalized ionic liquid membranes for CO_2 separation. *Chem. Commun.* **2018**, *54*, 12671−12685.
(16) Klemm, A.; Lee, Y.-Y.; Mao, H.; Gurkan, B. Facilitated Transport Membranes With Ionic Liquids for CO_2 Separations. *Front. Chem.* **2020**, *8*, 637.
(17) Hanioka, S.; Maruyama, T.; Sotani, T.; Teramoto, M.; Matsuyama, H.; Nakashima, K.; Hanaki, M.; Kubota, F.; Goto, M. CO_2 separation facilitated by task-specific ionic liquids using a supported liquid membrane. *J. Membr. Sci.* **2008**, *314*, 1−4.
(18) Kasahara, S.; Kamio, E.; Ishigami, T.; Matsuyama, H. Amino acid ionic liquid-based facilitated transport membranes for CO_2 separation. *Chem. Commun.* **2012**, *48*, 6903−6905.
(19) Kasahara, S.; Kamio, E.; Ishigami, T.; Matsuyama, H. Effect of water in ionic liquids on CO_2 permeability in amino acid ionic liquid-based facilitated transport membranes. *J. Membr. Sci.* **2012**, *415*−*416*, 168−175.
(20) Moghadam, F.; Kamio, E.; Matsuyama, H. High CO_2 separation performance of amino acid ionic liquid-based double network ion gel membranes in low CO_2 concentration gas mixtures under humid conditions. *J. Membr. Sci.* **2017**, *525*, 290−297.
(21) Kasahara, S.; Kamio, E.; Otani, A.; Matsuyama, H. Fundamental Investigation of the Factors Controlling the CO_2 Permeability of Facilitated Transport Membranes Containing Amine-Functionalized Task-Specific Ionic Liquids. *Ind. Eng. Chem. Res.* **2014**, *53*, 2422−2431.
(22) Santos, E.; Albo, J.; Irabien, A. Acetate based Supported Ionic Liquid Membranes (SILMs) for CO_2 separation: Influence of the temperature. *J. Membr. Sci.* **2014**, *452*, 277−283.
(23) Huang, K.; Zhang, X.-M.; Li, Y.-X.; Wu, Y.-T.; Hu, X.-B. Facilitated separation of CO_2 and SO_2 through supported liquid membranes using carboxylate-based ionic liquids. *J. Membr. Sci.* **2014**, *471*, 227−236.
(24) Makino, T.; Umecky, T.; Kanakubo, M. CO_2 Absorption Properties and Mechanisms for 1-Ethyl-3-methylimidazolium Ether-Functionalized Carboxylates. *Ind. Eng. Chem. Res.* **2016**, *55*, 12949−12961.
(25) Niedermeyer, H.; Hallett, J. P.; Villar-Garcia, I. J.; Hunt, P. A.; Welton, T. Mixtures of ionic liquids. *Chem. Soc. Rev.* **2012**, *41*, 7780−7802.
(26) Karadağ, A.; Destegül, A. N-(2-hydroxyethyl)-ethylenediamine-based ionic liquids: Synthesis, structural characterization, thermal, dielectric and catalytic properties. *J. Mol. Liq.* **2013**, *177*, 369−375.
(27) Makino, T.; Kanakubo, M.; Umecky, T.; Suzuki, A. CO_2 solubility and physical properties of N-(2-hydroxyethyl)pyridinium bis(trifluoromethanesulfonyl)amide. *Fluid Phase Equilib.* **2013**, *357*, 64−70.
(28) Fujii, K.; Makino, T.; Hashimoto, K.; Sakai, T.; Kanakubo, M.; Shibayama, M. Carbon Dioxide Separation Using a High-toughness Ion Gel with a Tetra-armed Polymer Network. *Chem. Lett.* **2015**, *44*, 17−19.
(29) Gurau, G.; Rodríguez, H.; Kelley, S. P.; Janiczek, P.; Kalb, R. S.; Rogers, R. D. Demonstration of Chemisorption of Carbon Dioxide in 1,3-Dialkylimidazolium Acetate Ionic Liquids. *Angew. Chem., Int. Ed.* **2011**, *50*, 12024−12026.
(30) Kortunov, P. V.; Siskin, M.; Baugh, L. S.; Calabro, D. C. In Situ Nuclear Magnetic Resonance Mechanistic Studies of Carbon Dioxide Reactions with Liquid Amines in Non-aqueous Systems: Evidence for the Formation of Carbamic Acids and Zwitterionic Species. *Energy Fuels* **2015**, *29*, 5940−5966.
(31) Kortunov, P. V.; Baugh, L. S.; Siskin, M. Pathways of the Chemical Reaction of Carbon Dioxide with Ionic Liquids and Amines in Ionic Liquid Solution. *Energy Fuels* **2015**, *29*, 5990−6007.
(32) Johnson, O.; Joseph, B.; Kuhn, J. N. CO_2 separation from biogas using PEI-modified crosslinked polymethacrylate resin sorbent. *J. Ind. Eng. Chem.* **2021**, *103*, 255−263.
(33) Arcis, H.; Coulier, Y.; Ballerat-Busserolles, K.; Rodier, L.; Coxam, J.-Y. Enthalpy of Solution of CO_2 in Aqueous Solutions of Primary Alkanolamines: A Comparative Study of Hindered and Nonhindered Amine-Based Solvents. *Ind. Eng. Chem. Res.* **2014**, *53*, 10876−10885.
(34) Comesaña-Gándara, B.; Chen, J.; Bezzu, C.; Carta, M.; Rose, I.; Ferrari, M.-C.; Esposito, E.; Fuoco, A.; Jansen, J. C.; McKeown, N. B. Redefining the Robeson upper bounds for CO_2/CH_4 and CO_2/N_2 separations using a series of ultrapermeable benzotriptycene-based polymers of intrinsic microporosity. *Ener. Environ. Sci.* **2019**, *12*, 2733−2740.

https://doi.org/10.1021/acsomega.2c04756
ACS Omega 2022, 7, 42155−42162